Commun Nonlinear Sci Numer Simulat 17 (2012) 4336–4345

Contents lists available at SciVerse ScienceDirect

Commun Nonlinear Sci Numer Simulat

journal homepage: www.elsevier.com/locate/cnsns

Transient chaos and crisis phenomena in butterfly valves driven by solenoid actuators

Peiman Naseradinmousavi [1], C. Nataraj *

Department of Mechanical Engineering, Center for Nonlinear Dynamics and Control, Villanova University, Villanova, 19085 PA, USA

ARTICLE INFO

Article history:
Received 28 September 2011
Received in revised form 29 January 2012
Accepted 30 January 2012
Available online 25 February 2012

Keywords:
Chaos
Crisis
Nonlinear modeling
Nonlinear dynamics
Butterfly valve
Solenoid actuator
Smart valves

ABSTRACT

Chilled water systems used in the industry and on board ships are critical for safe and reliable operation. It is hence important to understand the fundamental physics of these systems. This paper focuses in particular on a critical part of the automation system, namely, actuators and valves that are used in so-called "smart valve" systems. The system is strongly nonlinear, and necessitates a nonlinear dynamic analysis to be able to predict all critical phenomena that affect effective operation and efficient design. The derived mathematical model includes electromagnetics, fluid mechanics, and mechanical dynamics. Nondimensionalization has been carried out in order to reduce the large number of parameters to a few critical independent sets to help carry out a broad parametric analysis. The system stability analysis is then carried out with the aid of the tools from nonlinear dynamic analysis. This reveals that the system is unstable in a certain region of the parameter space. The system is also shown to exhibit crisis and transient chaotic responses; this is characterized using Lyapunov exponents and power spectra. Knowledge and avoidance of these dangerous regimes is necessary for successful and safe operation.

1. Introduction

Modeling and designing accurate shipboard machinery systems has received much attention as one of the important challenges that needs to be overcome for supporting the next generation Naval machinery automation requirements. Typical automation systems used in the US Navy consist of actuators, sensors, controllers, valves, piping, electrical cabling and communication wiring. Many types of actuator-valve systems are in use [1,2].

In general, these systems are nonlinear and exhibit nonlinear phenomena such as multiple steady solutions, bifurcations, multi-frequency responses, and chaotic dynamics. All of these phenomena have been observed in practice but cannot be explained even qualitatively by traditional linear theories used in engineering practice.

This paper focuses in particular on a critical part of the automation system, namely, actuator-valve systems that form an important part of what are termed "smart valve" systems. All of these systems are nonlinear and need to be analyzed as such. Nonlinear dynamic analysis of such an interdisciplinary system is not trivial, but needs to be investigated in order to predict possible critical phenomena including chaos and its routes.

Specific work related to the system considered here is somewhat difficult to find; however, there has certainly been much research in related areas and is discussed here. Important nonlinear phenomena in electromechanical systems such as chaos have received considerable attention by researchers. Belato et al. [3] analyzed chaotic vibrations of an electromechanical system which includes a nonlinear dynamic system consisting of a simple pendulum whose support point is vibrated along

* Corresponding author. Tel.: +1 610 519 4994.
E-mail addresses: pnaser01@villanova.edu (P. Naseradinmousavi), nataraj@villanova.edu (C. Nataraj).
[1] Tel.: +1 484 804 0384.

1007-5704/$ - see front matter © 2012 Elsevier B.V. All rights reserved.
doi:10.1016/j.cnsns.2012.01.034

Nomenclature

α	valve rotation angle
ΔP	pressure drop across the valve
Δt	time step for numerical integration
μ	friction coefficient of the bearing area
ρ	fluid density
c	damping coefficient
C_s	coefficient of the seating area
C_{cc}	sum of upper and lower contraction coefficients
D_s	diameter of the valve shaft
D_v	pipe diameter
F_c	action and reaction forces of the rack and pinion
F_m	magnetic actuation force
g_0	maximum stroke of the solenoid plunger
i	applied current
J	mass moment inertia of the disk
k	spring stiffness
m	mass of the plunger
N	number of coils
r	radius of pinion
R_1	sum of reluctances of the magnetic flux paths excluding airgap
R_2	reluctance of the airgap
T_b	bearing torque
T_c	hydrodynamic torque coefficient which can be calculated by a table look up for various values of α
T_h	hydrodynamic torque
T_s	seating torque
V	supply voltage
V_0	inlet velocity of flow
V_J	jet velocity
x	displacement of the solenoid plunger

a horizontal guide by a two bar linkage driven by a DC motor with limited power. Nonlinear dynamic analysis of a micro electromechanical system (MEMS) has been carried out by Xie et al. [4] based on an invariant manifold method proposed by Boivin et al. [5]. Ge and Lin [6] have studied dynamical analysis of electromechanical gyrostat system subjected to external disturbance.

Chaotic responses are distinguishable by sensitivity to initial conditions which are examined in this paper. Power spectra and Lyapunov exponents are also helpful to identify chaotic system responses since they exhibit a broadband power spectrum, and one or more positive Lyapunov exponents must be observed [7]. In particular, we are interested in transient chaos, which can be found in many systems whose asymptotic behavior is regular [8], but they exhibit extreme sensitivity to initial conditions, which is characteristic of chaos. The important difference is that it survives only for a finite time. Such phenomena involved with finite time intervals are complex and difficult to discover and characterize.

The first part of the paper deals with a high-fidelity mathematical model, and the second part deals with nonlinear dynamic analysis of the system. This paper follows on the previous work carried out by the authors [9].

2. Mathematical modeling

The system consists of a solenoid actuator energized by an electric voltage (DC or AC) which moves a plunger. The plunger is connected to a butterfly valve through a rack and pinion arrangement as shown in Fig. 1. The magnetic flux generates the needed electromagnetic force to move the plunger and subsequently results in the rotation of the butterfly valve by the coupled rack and pinion mechanism.

An ideal pressure angle is assumed for the rack and pinion mechanism with an assumption of no backlash of the gears. The valve controls the flow in a pipe and is hence subject to hydrodynamic forces.

2.1. Electromagnetics

The magnetic force is calculated using the reluctance method [9] as follows.

$$F_m = \frac{R_2 N^2 i^2}{2(R_1 + R_2(g_0 - x))^2} \tag{1}$$

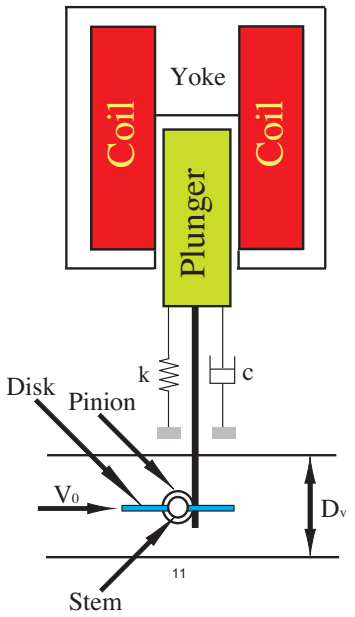

Fig. 1. Schematic model of the system.

A simple circuit model leads to the following nonlinear mathematical model. The inverse function nonlinearity, in particular, defies easy linearization.

$$\frac{di}{dt} = \frac{(V - Ri)(R_1 + R_2(g_0 - x))}{N^2} - \frac{R_2 i\dot{x}}{(R_1 + R_2(g_0 - x))} \tag{2}$$

2.2. Fluid mechanics

Analysis must be done on the hydrodynamic, bearing, and seating torques as they are highly nonlinear functions affecting the valve rotation angle. The torque terms are given as follows [10–14].

$$T_h = \frac{8\rho T_c D_v^3 V_0^2}{3\pi} \underbrace{\frac{4}{[C_{cc}(1-\sin\alpha)]^2}}_{\left(\frac{V_J}{V_0}\right)^2} \tag{3}$$

$$T_b = \frac{\pi}{8}\mu D_s D_v^2 \Delta P \,\mathrm{sign}(\dot{\alpha}) \tag{4}$$

$$T_s = C_s D_v^2 \tag{5}$$

Figs. 2 and 3 illustrate variations of T_c and C_{cc}, respectively, vs. α. The pressure drop across the valve is calculated as follows.

$$\Delta P = \frac{1}{2}\rho V_0^2 \left(\frac{V_J}{V_0} - 1\right)^2 \tag{6}$$

Clearly, the hydrodynamic and bearing torques are strongly nonlinear functions of the valve angle.

2.3. Dynamics

The dynamical equations of the plunger and butterfly valve can be written as follows (Fig. 4).

$$m\ddot{x} + c\dot{x} + kx = F_m - F_c \tag{7}$$

$$J\ddot{\alpha} + b\dot{\alpha} = rF_c + T_h - T_b - T_s \tag{8}$$

In addition, we have the kinematic constraint between the rack and the pinion,

$$x = r\alpha. \tag{9}$$

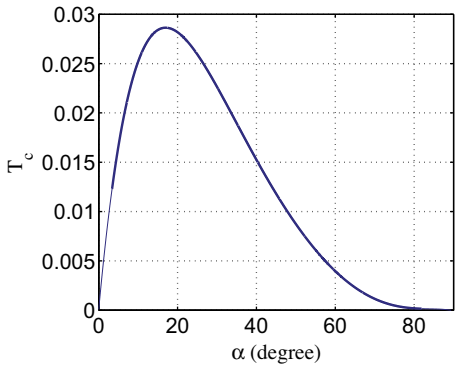

Fig. 2. Hydrodynamic torque coefficient vs. α.

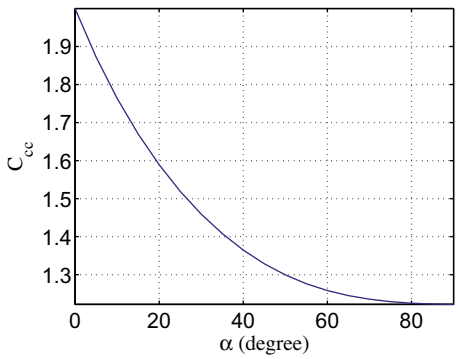

Fig. 3. C_{cc} vs. α.

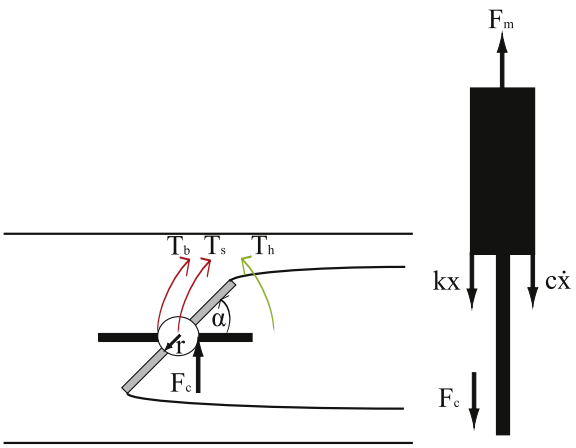

Fig. 4. Free body diagrams of the solenoid actuator and the butterfly valve.

Combining Eqs. (1), (3)–(5), (7), (and) (8), one has,

$$(mr^2+J)\ddot{\alpha}+(cr^2+b)\dot{\alpha}+kr^2\alpha=\frac{rR_2N^2i^2}{2(R_1+R_2(g_0-r\alpha))^2}+\frac{32\rho T_cD_v^3V_0^2}{3\pi[C_{cc}(1-\sin(\alpha))]^2}-\frac{\pi}{16}\mu\rho D_sD_v^2V_0^2\ \text{sign}\ (\dot{\alpha})\left(\frac{2}{C_{cc}(1-\sin(\alpha))}-1\right)^2-C_sD_v^2 \tag{10}$$

Note that C_{cc} and T_c are dependent on α. Eqs. (2) and (10) constitute the third order dynamic model for the system.

3. Nondimensionalization

In order to reduce the number of parameters, and to perform a systematic analysis, the nonlinear dynamic equations need to be nondimensionalized. We define the state vector as $x = [\alpha, \dot{\alpha}, i]^T$, and derive the nondimensionalized state-space equations as follows.

$$\dot{x}_1 = x_2 \tag{11}$$

$$\dot{x}_2 = -x_1 - 2\zeta x_2 + \frac{\vartheta x_3^2}{(\Delta_1 + \Delta_2(\gamma - x_1))^2} + (x_1(\beta_1 e^{a x_1} + \beta_2)) - \mathrm{sign}(x_2)\left(\kappa_1 x_1^2 e^{\kappa_2 x_1} + \kappa_3 e^{\kappa_4 x_1}\right) - \frac{C_s D_v^2}{\omega_{n0}^2 (J + mr^2)} \tag{12}$$

$$\dot{x}_3 = \frac{(v - x_3)(\Delta_1 + \Delta_2(\gamma - x_1))}{N^2} - \frac{\Delta_2 x_2 x_3}{(\Delta_1 + \Delta_2(\gamma - x_1))} \tag{13}$$

Here,

$$\omega_{n0} = \sqrt{\frac{kr^2}{J + mr^2}}; \quad \gamma = \frac{g_0}{r}; \quad \Delta_1 = \frac{RR_1}{\omega_{n0}}; \quad \Delta_2 = \frac{RR_2 r}{\omega_{n0}}$$

$$\zeta = \frac{(b + cr^2)}{2\omega_{n0}(J + mr^2)}; \quad \vartheta = \frac{rR_2 N^2 i_0^2 R^2}{2\omega_{n0}^4 (J + mr^2)}$$

The values of β_1, β_2, a, κ_1, κ_2, κ_3 and κ_4 are calculated based on fitting the torques (in nondimensional form) to the following functions with least square error.

$$T_h = \beta_1 \alpha e^{a\alpha} + \beta_2 \alpha \tag{14}$$

$$T_b = \kappa_1 \alpha^2 e^{\kappa_2 \alpha} + \kappa_3 e^{\kappa_4 \alpha} \tag{15}$$

4. Nonlinear analysis

The model has twelve nondimensional parameters; the analysis presented in this paper assumes specific values for ten of them as shown in Table 1; these values are based on realistic parameter values for an industrial system. Two parameters, ϑ and ζ are considered to vary over a range of values.

The sign function is replaced by a differentiable function to make the linearization process easier. A smooth approximation of the sign function is,

$$\mathrm{sign}(x_2) \approx \tanh(Kx_2) \tag{16}$$

where, K can be tuned to get a good approximation; we used $K = 1$ in this analysis.

The Jacobian matrix for the system can be calculated as follows.

$$J = \begin{bmatrix} 0 & 1 & 0 \\ A_0 & A_1 & \frac{2\vartheta x_{30}}{(\Delta_1 + \Delta_2(\gamma - x_{10}))^2} \\ B_0 & -\frac{\Delta_2 x_{30}}{(\Delta_1 + \Delta_2(\gamma - x_{10}))} & C_0 \end{bmatrix} \tag{17}$$

Table 1
Nondimensional parameters.

β_1	7×10^{-4}	a	5.2764
β_2	0.44	γ	1.8
κ_1	1×10^{-7}	κ_2	13.62
κ_3	−0.5	ζ	Varies
κ_4	−13	ϑ	Varies
Δ_1	536	Δt	10^{-4}
Δ_2	1×10^4		

where,

$$A_0 = \frac{2\vartheta x_{30}^2 \Delta_2}{(\Delta_1 + \Delta_2(\gamma - x_{10}))^3} + \beta_1 e^{\alpha x_{10}}(1 + \alpha x_{10}) + \beta_2 - 1 \tag{18}$$

$$A_1 = -2\zeta - K(1 - \tanh^2 K x_{20})(\kappa_1 x_{10}^2 e^{\kappa_2 x_{10}} + \kappa_3 e^{\kappa_4 x_{10}}) \tag{19}$$

$$B_0 = -\frac{\Delta_2(\upsilon - x_{30})}{N^2} - \frac{\Delta_2^2 x_{20} x_{30}}{(\Delta_1 + \Delta_2(\gamma - x_{10}))^2} \tag{20}$$

$$C_0 = -\frac{\Delta_1 + \Delta_2(\gamma - x_{10})}{N^2} - \frac{\Delta_2 x_{20}}{\Delta_1 + \Delta_2(\gamma - x_{10})} \tag{21}$$

and $[x_{10}, x_{20}, x_{30}]$ is an equilibrium point of the system.

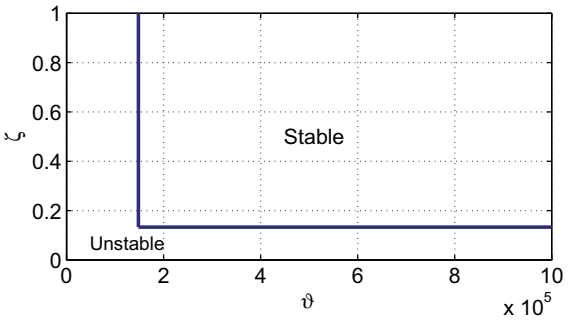

Fig. 5. Stability map in the (ζ and ϑ) parameter plane.

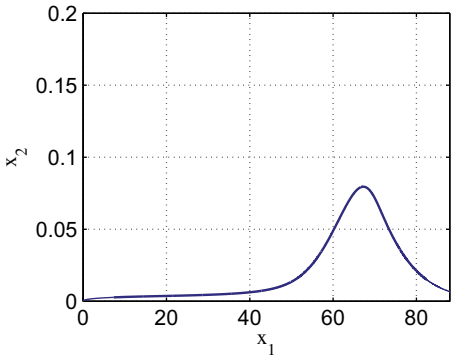

Fig. 6. The system response for $\zeta = 0.5$ and $\vartheta = 4.8 \times 10^5$.

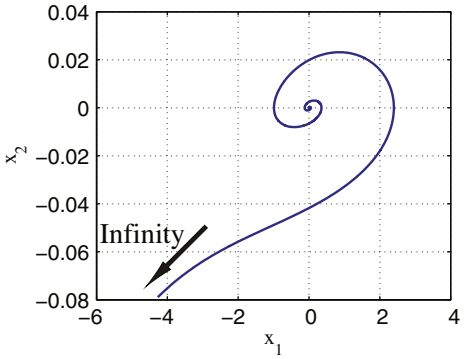

Fig. 7. The system response for $\zeta = 0.05$ and $\vartheta = 1 \times 10^3$.

For the linearized system, the characteristic equation becomes

$$s^3 + \left(2\zeta + \frac{\Delta_1 + \Delta_2(\gamma - x_{10})}{N^2} + K\left(\kappa_1 x_{10}^2 e^{\kappa_2 x_{10}} + \kappa_3 e^{\kappa_4 x_{10}}\right)\right)s^2 + \left(\left(2\zeta + K\left(\kappa_1 x_{10}^2 e^{\kappa_2 x_{10}} + \kappa_3 e^{\kappa_4 x_{10}}\right)\right) \times \left(\frac{\Delta_1 + \Delta_2(\gamma - x_{10})}{N^2}\right) + 1 - \left(\beta_1 e^{\alpha x_{10}}(1 + \alpha x_{10}) + \beta_2\right)\right)s + A_0 C_0 = 0. \tag{22}$$

Using Routh–Hurwitz criteria, one is able to judge the system's linear stability behavior. The asymptotical stability requirements of the system can then be determined as follows.

$$\frac{2\vartheta x_{30}^2 \Delta_2}{(\Delta_1 + \Delta_2(\gamma - x_{10}))^3} + \beta_1 e^{\alpha x_{10}}(1 + \alpha x_{10}) + \beta_2 < 1 \tag{23}$$

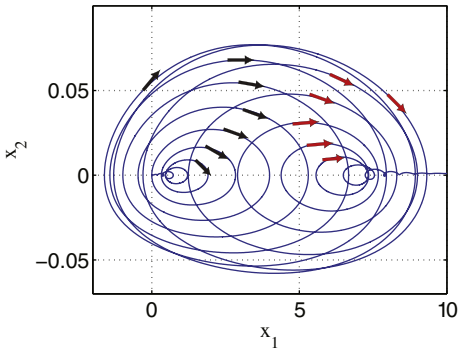

Fig. 8. Phase portrait for $\zeta = 0.133$ and $\vartheta = 1.48 \times 10^5$.

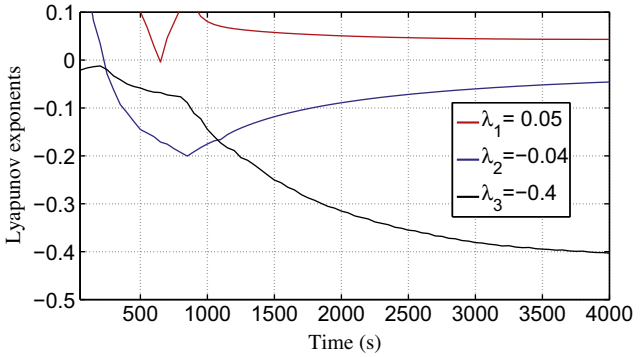

Fig. 9. Lyapunov exponents for $\zeta = 0.133$ and $\vartheta = 1.48 \times 10^5$.

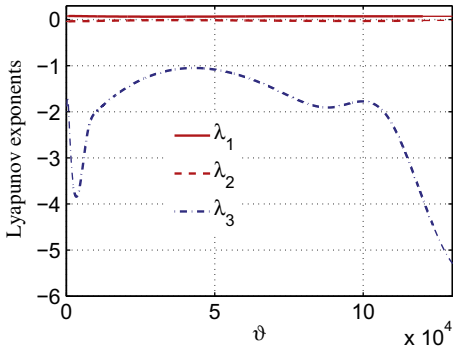

Fig. 10. Lyapunov exponents vs. ϑ for $\zeta = 0.133$.

$$\frac{4\zeta^2(\Delta_1+(\gamma-x_{10})\Delta_2)}{N^2}+\frac{2\zeta(\Delta_1+(\gamma-x_{10})\Delta_2)^2}{N^4}+\frac{2\vartheta x_{30}^2\Delta_2}{N^2(\Delta_1+(\gamma-x_{10})\Delta_2)^2}+4\zeta K\left(\kappa_1x_{10}^2e^{\kappa_2x_{10}}\kappa_3e^{\kappa_4x_{10}}\right)$$
$$\times\frac{(\Delta_1+(\gamma-x_{10})\Delta_2)}{N^2}+2\zeta+K\left(\kappa_1x_{10}^2e^{\kappa_2x_{10}}+\kappa_3e^{\kappa_4x_{10}}\right)\times\frac{(\Delta_1+(\gamma-x_{10})\Delta_2)^2}{N^4}+K^2\left(\kappa_1x_{10}^2e^{\kappa_2x_{10}}+\kappa_3e^{\kappa_4x_{10}}\right)^2$$
$$\times\frac{(\Delta_1+(\gamma-x_{10})\Delta_2)}{N^2}+K\left(\kappa_1x_{10}^2e^{\kappa_2x_{10}}+\kappa_3e^{\kappa_4x_{10}}\right)$$
$$>2\zeta(\beta_1e^{ax_{10}}(1+ax_{10})+\beta_2)+K\left(\kappa_1x_{10}^2e^{\kappa_2x_{10}}+\kappa_3e^{\kappa_4x_{10}}\right)\times(\beta_1e^{ax_{10}}(1+ax_{10})+\beta_2) \quad (24)$$

It can be shown from Eq. 23 that the system reveals an unstable response unless k is large enough to reduce the value of β_2. Eq. 24 yields a comprehensive relationship to examine the system stability by varying the critical parameters such as ζ (equivalent viscous damping) and ϑ (magnetic force parameter).

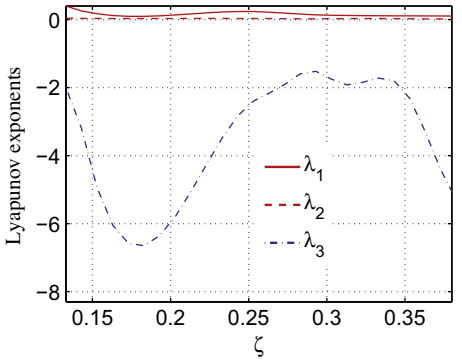

Fig. 11. Lyapunov exponents vs. ζ for $\vartheta = 5\times10^3$.

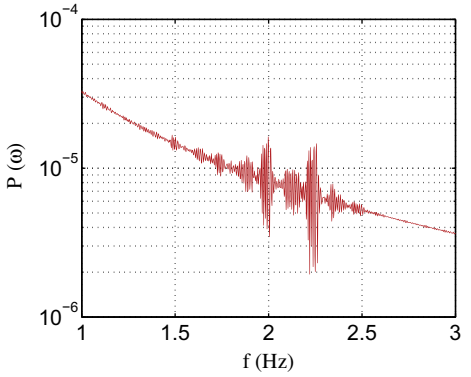

Fig. 12. Power spectrum for $\zeta = 0.133$ and $\vartheta = 1.48\times10^5$.

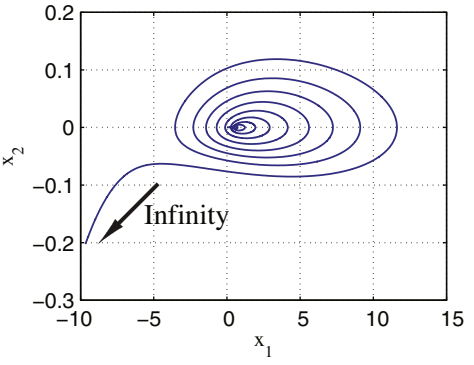

Fig. 13. Phase portrait for $\zeta = 0.1329$ and $\vartheta = 1.48\times10^5$.

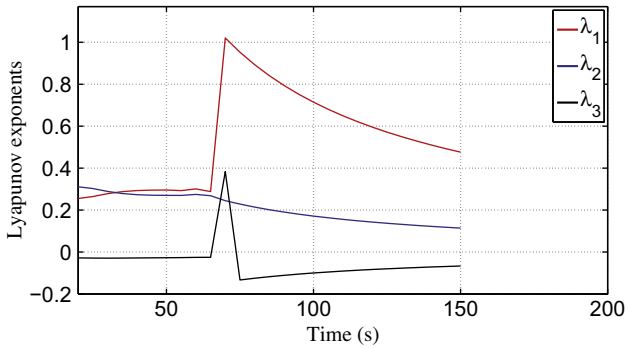

Fig. 14. Lyapunov exponents for $\zeta = 0.1329$ and $\vartheta = 1.48 \times 10^5$.

Fig. 5 illustrates the range of ζ vs. ϑ obtained from the stability criteria from which the stable and unstable regions can be distinguished. A confirmation of the stability map is shown in Fig. 6 revealing the stable behavior of the system for $\zeta = 0.5$ and $\vartheta = 4.8 \times 10^5$; the system's unstable behavior can be observed from Fig. 7 where the response diverges to infinity. We will also investigate a set of unstable values of ζ and ϑ to evaluate the system behavior at their critical values in the sense of fixing ζ with varying ϑ, and vice versa.

The transient motion appears to have the characteristics of a strange attractor, but eventually settles into a regular motion. It exhibits narrow-band chaos, a chaotic motion whose phase space orbits remain close to some periodic or regular orbit; in general, such spectra often show narrow or limited broadening of certain frequency spikes. Shown in Fig. 8 is this transient chaotic motion trapped between two regular motions for a marginal value of ζ. The response confirms the occurrence of finite time chaos and approaches a regular motion eventually.

The Lyapunov exponents of such a motion shown in Fig. 9 confirm the observed chaotic motion; one positive Lyapunov exponent is distinguishable. Note that the positive value is not big enough to yield a chaotic motion forever and its effects finally will be mitigated by the largest negative value of the Lyapunov exponents ($|\lambda_3| \approx 10|\lambda_1|$). Figs. 10 and 11 also illustrate the variations of Lyapunov exponents vs. ζ and ϑ and confirm it. We used an integration time step of 10^{-4} second. Shown in Fig. 12 is the power spectrum indicating the noisy characteristic typical of transient chaotic responses for a certain range of frequencies.

Zeeman [15] defines a catastrophe to be any discontinuous bifurcation. Abraham and Stewart [16] have been more specific and define blue sky catastrophe – a bifurcation in which an entire attractor disappears abruptly from the phase portrait as a control parameter α passes through its critical value α_c; when such a bifurcation occurs, the dynamical system will make a finite jump to a remote attractor, or diverge to infinity [17].

A small change in the critical value of ζ (0.133) yields the crisis phenomenon shown in Fig. 13 where a chaotic attractor abruptly disappears for $\zeta = 0.1329$ and diverges to infinity. It can also be validated from Fig. 14 where its Lyapunov exponents, having at least one positive value for a chaotic motion, suddenly disappear.

5. Conclusion

This paper employed recently developed accurate nonlinear dynamic models of butterfly valves operated by solenoid actuators. Many tools from nonlinear dynamic analysis were then utilized to investigate the system stability and distinguish between the responses for a set of parameters.

The variations of two critical parameters, ζ and ϑ, were then studied to establish stability regimes and to investigate harmful nonlinear phenomena such as chaos and crisis.

Lyapunov exponents were calculated displaying one positive value and the power spectrum showed a noisy nature confirming the chaotic nature of the response for a certain period of time. Also observed for some parametric value was a blue sky catastrophe phenomenon, which is distinguishable by the disappearance of a chaotic attractor and its divergence to infinity when the control parameter passes through its critical value.

Determining the critical range of these parameters is an important step that needs to be taken for safe operation of the system. Current work is focusing on experimental validation of these theoretical results.

Acknowledgment

This work was supported by Office of Naval Research Grant (N00014/08/1/0435). The authors are grateful to ONR, and Mr. Anthony Seman III in particular, for the financial support that made this research possible. Thanks are also due to Dr. Stephen Mastro and Mr. Frank Ferrese of Naval Surface Warfare Center (Philadelphia) for valuable help and guidance.

References

[1] Ryan Hughes, Santiago Balestrini, Kristin Kelly, Neil Weston, Dimitri Mavris. Modeling of an integrated reconfigurable intelligent system (IRIS) for ship design. In: Proceedings of the 2006 ASNE Ship and Ship Systems Technology (S3T) Symposium, 2006.
[2] Lequesne B, Henry R, Kamal M, Magnavalve: a new solenoid configuration based on a spring-mass oscillatory system for engine valve actuation. GM Research Report E3-89, June 1998.
[3] Belato D, Weber HI, Balthazar JM, Mook DT. Chaotic vibrations of a nonideal electro-mechanical system. Int J Solids Struct 2001;38(10-13):1699–706.
[4] Xie WC, Lee HP, Lim SP. Nonlinear dynamic analysis of MEMS switches by nonlinear modal analysis. J Nonlinear Dyn 2003;31(3):243–56.
[5] Boivin Nicolas, Pierre Christophe, Shaw Steven W. Non-linear normal modes, invariance, and modal dynamics approximations of non-linear systems. J Nonlinear Dyn 1995;8(3):315–46.
[6] Ge ZM, Lin TN. Chaos, chaos control and synchronization of electro-mechanical gyrostat system. J Sound Vibr 2003;259(3):585–603.
[7] Nayfeh Ali Hasan, Balachandran Balakumar. Applied nonlinear dynamics: analytical, computational, and experimental methods. Germany: Wiley VCH Verlag GmbH; 1995.
[8] Stefanski K, Buszko K, Piecyk K. Transient chaos measurements using finite-time Lyapunov exponents. Chaos 2010;20:033117. 1–13.
[9] Naseradinmousavi Peiman, Nataraj C. Nonlinear mathematical modeling of butterfly valves driven by solenoid actuators. J Appl Math Model 2011;35(5):2324–35.
[10] Park Ju Yeop, Chung Myung Kyoon. Study on hydrodynamic torque of a butterfly valve. J Fluids Eng 2006;128(1):190–5.
[11] Sarpkaya Turgut. Oblique impact of a bounded stream on a plane lamina. J Frankl Inst 1959;267(3):229–42.
[12] Sarpkaya Turgut. Torque and cavitation characteristics of butterfly valves. J Appl Mech 1961;28(4):511–8.
[13] Ogawa Kazuhiko, Kimura Takeyoshi. Hydrodynamic characteristics of a butterfly valve – prediction of torque characteristics. ISA Trans 1995;34(4):327–33.
[14] Leutwyler Z, Dalton C. A CFD study of the flow field, resultant force, and aerodynamic torque on a symmetric disk butterfly valve in a compressible fluid. J Pressure Vessel Tech 2008;130(2).
[15] Zeeman EC. Bifurcation and catastrophe theory. Papers Alg Anal Statist 1981;9:207–72.
[16] Abraham Ralph H, Bruce Stewart H. A chaotic blue sky catastrophe in forced relaxation oscillations. Physica D 1986;21:394–400.
[17] Stewart HB, Thompson JMT. Towards a classification of generic bifurcations in dissipative dynamical systems. Dyn Stability Syst 1986;1(1).